High-resolution optical study of a point-contact-induced phonon hot spot in ruby

K. Z. Troost, M. J. van Dort, J. I. Dijkhuis, and H. W. de Wijn
Faculty of Physics and Astronomy, and Debye Research Institute, University of Utrecht, P.O. Box 80000, 3508 TA Utrecht, The Netherlands
(Received 30 July 1990)

A phonon hot spot is generated in ruby at 1.5 K by a micrometer-sized whisker-film W-W point contact, and subsequently studied by means of high-resolution optical techniques. The phonon distribution in the immediate vicinity of the point contact is imaged directly with micrometer spatial resolution. The method used is to observe the R_1 luminescence following optical excitation of Cr^{3+} to $\bar{E}(^2E)$, where advantage is taken of the temperature dependence of the frequency and width of the $^4A_2-\bar{E}(^2E)$ optical transition. A model description of the propagating phonon distribution is presented in terms of classical heat conduction close to the point contact and of quasiballistic propagation further away. Results of numerical calculations of the space- and frequency-dependent phonon distribution agree well with experiment.

I. INTRODUCTION

In the past decade there has been substantial interest in the evolution of small-sized strongly thermally excited regions in semiconductors and insulators at low temperatures.[1,2] Strong local thermal excitation was first observed by Hensel and Dynes,[3] who used 10–100-μJ pulses from a Nd:YAG laser focused onto a metalized end of a Ge sample. They concluded that the temperature below the focus rose so high that the generated phonons no longer propagated ballistically, as they do in the case of a heat pulse, but diffusively: "In other words, there is an entrapment of phonons creating a localized 'hot spot'."

Up till now, most of the experiments on hot spots have been performed in semiconductors at low temperatures. The techniques involved either the use of direct optical interband excitation of electrons, which creates zone-boundary acoustic phonons during ultrafast nonradiative relaxation to the band edge,[3–7] or optical excitation of a metallic film evaporated onto one of the crystal faces.[3,8,9] Phonon detection has been performed with a bolometer,[3,4,8] via exciton luminescence,[6,7,9] or by use of the luminescent properties of a thin crystalline film deposited on the specimen.[5] From these experiments it has been established that hot spots have lifetimes of the order of microseconds. Furthermore, nonequilibrium phonon distributions have been found, particularly of subterahertz phonons with subthermal occupations, and of trapped high-frequency phonons with above-thermal occupations. Experiments on hot spots in insulators have been performed by Bron *et al.*[10] and Abramov *et al.*[11] To generate a hot spot, the latter authors used 10-μJ pulses from a Constantan heater evaporated onto a $CaF_2:Eu^{2+}$ crystal. Tunable frequency-resolved phonon detection was achieved via the luminescence from the upper sublevel of the piezospectroscopically split Γ_8^+ level of the $4f5d$ configuration of Eu^{2+}, as devised by Eisfeld and Renk.[12] A hot-spot temperature of 17 K was reached in a volume of about 1 mm^3.

In this paper we present the results and an analysis of experiments on a hot spot in dilute ruby ($Al_2O_3:Cr^{3+}$). To achieve a size of only a few micrometers, the hot spots were generated with a metallic whisker-film point contact. The small size of point contacts further permits the injection into the crystal of exceptionally high power fluxes with only moderate electrical power (up to 3×10^{10} W/m^2 at 1 W). A 1-W quasistationary pulse of 3-μs duration, for example, which results in an energy dissipation of only 3 μJ, is, under adiabatic conditions, sufficient to heat ruby to temperatures up to 1000 K over the typical volume of the hot spot (a hemisphere with a radius of order 10 μm).[13] Note in this context that in Al_2O_3 at low temperatures elastic phonon scattering is weak. Ruby further permits high-resolution spectroscopic techniques to be used to detect the phonons in the hot spot as well as the phonons that have escaped from it. Because the $\bar{E}(^2E)$ level shifts toward lower energy with increasing phonon occupation, these techniques allow one to determine at what distance from the point contact a given phonon occupation is established. High spectral resolution is in this way converted into high spatial resolution. A spatial resolution of a few μm can, in fact, be achieved. Thermal phonons are removed by cooling to 1.5 K.

In the analysis, a model, resembling a qualitative analytical treatment by Kozub,[14] is worked out in detail. In the immediate vicinity of the point contact, heat transport is assumed to take place by classical heat conduction. The size of the hot spot is accordingly related to the phonon mean free path. Outside the hot spot, the heat propagation is considered to be quasiballistic,[1] i.e., the ballistically propagating phonons are subjected to breakup and recombination by strongly frequency-dependent anharmonic scattering. In the quasiballistic region, the model has, for tractability, been formulated in terms of a finite number of discrete Einstein modes.[15]

II. METHOD

The phonon distribution is observed in a spatially resolved way by taking advantage of the shift of the

$\bar{E}(^2E)$ level toward lower energy with increasing phonon energy. Consider, as in Fig. 1, the position of the $\bar{E}(^2E)$ level of Cr^{3+} in a part of the crystal with a marked phonon occupation ("hot") with reference to Cr^{3+} not subjected to phonons ("cold"). In the hot part, the $\bar{E}(^2E)$ state is shifted toward lower energy by an amount δE, which scales with the phonon energy density.[16] Concomitantly, the phonon occupation invokes a homogeneous broadening of $\bar{E}(^2E)$, which at the phonon densities of interest here is however smaller than the line shift. A thermal phonon occupation corresponding to 100 K, for example, leads to $\delta E \sim 1\ cm^{-1}$, while the additional linewidth amounts to only $\Delta\nu \sim 0.2\ cm^{-1}$ FWHM. To selectively excite Cr^{3+} in the hot part of the crystal, therefore, we tune the narrow-band dye laser below the low-temperature $^4A_2 - \bar{E}(^2E)$ resonance frequency. In effect, all Cr^{3+} are excited that have δE's within a range of width $\Delta\nu$ centered around the laser frequency ν_l. The spatial extent of these Cr^{3+} may subsequently be measured by imaging the R_1 luminescence emitted upon their return to $^4A_2$. In this way high-frequency resolution is converted into high-spatial resolution. Note here that the luminescent area may be essentially smaller than the laser focus. Since the phonon density drops approximately quadratically with the distance from the point contact, the Cr^{3+} selected are in good approximation located in a hemispherical shell. The radius R of this shell as well as its thickness obviously increase with decreasing deviation $\delta\nu_l$ of the laser from resonance.

III. EXPERIMENTAL DETAILS

In the experiments, a Czochralsky-grown ruby crystal measuring $15\times10\times7\ mm^3$ was used. The crystal, immersed in liquid helium at 1.5 K, had a Cr^{3+} concentration of 700 at.ppm, and the c axis was perpendicular to the $15\times7\text{-}mm^2$ faces. The anvil of the point contact was formed by a 50-nm-thick W film, deposited on a polished $15\times7\text{-}mm^2$ face by dc sputtering with Kr at 10 kV. Prior to the deposition of the film, this face was cleaned with a glow discharge for half an hour. The spear of the point contact, a 100-μm diameter W wire soldered to a 1-mm-diameter Ni post serving as a mechanical support, was electrochemically etched to form a tip with a radius of typically 1 μm in a 1-mole NaOH solution with an ac current of 10 mA at 1 kHz. Instead of W-W point contacts, Au-Au point contacts with similar specifications were sometimes used. Precise vertical positioning of the whisker against the film was accomplished under liquid helium with a differential screw mechanism (50 μm/turn), operated from the top of the cryostat. The point contacts were electrically excited with dc voltages of up to 16 V. Superimposed negative pulses of 100-ns duration and 900-kHz repetition rate made it possible to measure the impedance of the point contact via their reflection back into the 50-Ω coaxial cable.

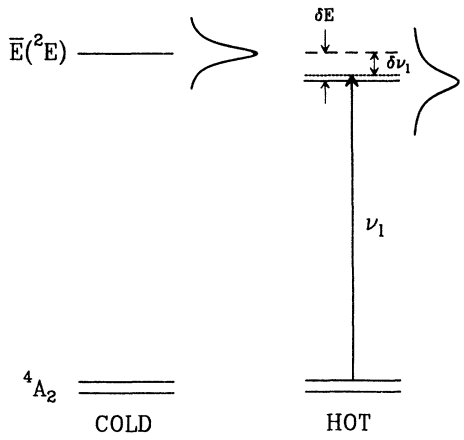

FIG. 1. The principle of direct temperature-selective laser excitation of $\bar{E}(^2E)$. Shift and broadening of $\bar{E}(^2E)$ toward higher temperatures are indicated schematically.

The temperature-selective optical excitation of Cr^{3+} centers below the point contact was achieved with a narrow-band ring dye laser (1 MHz spectral width, LD688 dye), pumped by an Ar ion laser operating in the all-lines mode. The laser beam was focused to a waist of 100 μm with a 50-mm camera lens, and directed toward the point contact from below, reflecting at an angle of approximately 20° with the film. The luminescence emanating from the detection zone was collected at right angles to the incoming laser beam with a 50-mm camera lens, and recorded with a video camera after magnification by a microscope objective. To ensure optical access, the crystal was mounted at an angle of 15°. The hot spot as viewed via the luminescence thus has the appearance of a complete sphere, being made up of the actual luminescent hemisphere plus its image reflected from the metal film. The spatial resolution of the optical imaging system, inclusive of the stability of the sample positioning in the cryostat, is estimated to be a few μm. The video images were subsequently digitized and transferred to a computer.

To illustrate the hot spot as seen via the luminescence, two of these images are shown in Fig. 2. Upon deriving the size of the luminescent zone from these images, it should be realized that the $^4A_2$ ground state is split into 2 Kramers doublets. These doublets, separated by 11.4 GHz, are populated about equally at 1.5 K. Obviously, for a given laser setting, the absorption arising from Cr^{3+} in the upper doublet ($M_S = \pm\frac{1}{2}$) corresponds to the smaller laser detuning $\delta\nu_l$, and accordingly to the luminescent region with the *larger* radius. The absorption from the lower doublet ($M_S = \pm\frac{3}{2}$), which is associated with an 11.4-GHz larger $\delta\nu_l$, however, tends to fill the darker central portion of the luminescent hemisphere. The relative weights of the contributions from $M_S = \pm\frac{1}{2}$ and $M_S = \pm\frac{3}{2}$, of course, depend on the linewidth as a function of phonon occupation, on the inhomogeneous broadening of $\bar{E}(^2E)$, and on the polarization of the incident laser beam. They further depend on the population ratio of the two ground doublets, which under the condition of a strong optical pumping cycle tends to deviate from the thermal value by virtue of the slowness of the spin-lattice relaxation within the $^4A_2$ state.[17] Another

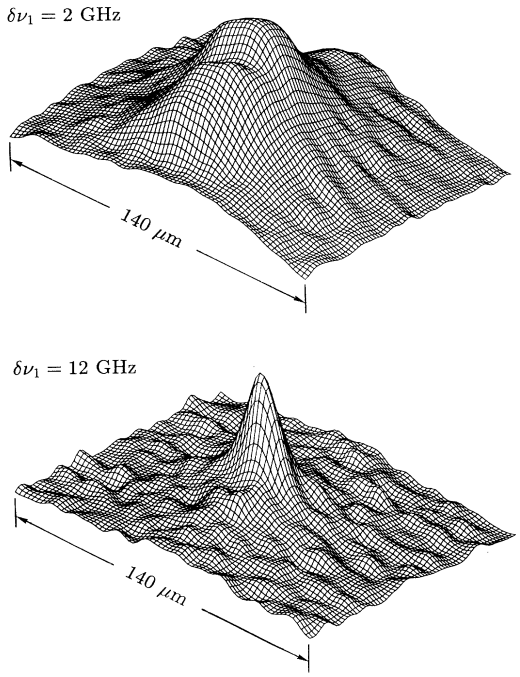

FIG. 2. Digitized video images of the spatial luminescence profiles below the point contact, for $\delta\nu_l = 2$ and 12 GHz, respectively. Point-contact power is 0.5 W.

difficulty is that the population ratio of the $^4A_2$ doublets may be substantially modified by interaction with the phonons emitted by the point contact itself.[18,19] To avoid the substantial complications of incorporating these effects as well as the ambiguities involved, we have simply adopted the definition that the extent of the luminescent region at half intensity refers to the $\delta\nu_l$ belonging to the *upper* $^4A_2$ doublet. For $\delta\nu_l = 12$ GHz, then, a luminescent region with a diameter of 22 μm at half intensity is found. Upon correcting for the spatial resolution, this yields a radius of 11 μm for the region with a phonon occupation characterized by $\delta\nu_l = 12$ GHz. Similarly, we find that a detuning $\delta\nu_l$ amounting to 2 GHz, i.e., a substantially lower phonon occupation such as prevails further away from the point contact, corresponds to a radius of 45 μm.

IV. PHONON DISTRIBUTION

In this section we set up a model to describe the phonon spectrum below the point contact as it evolves with distance. Following Kozub,[14] we distinguish two regimes of propagation away from the point contact. First, a hemisphere with a radius R_0 and a surface temperature T_0 is assumed to delimit the hot spot itself, i.e., the inner region where the phonon density is so high and the phonon mean free path so short that thermal equilibrium is established everywhere. In this regime the energy propagation is adequately described by classical heat conduction. In the regime outside the hemisphere, by contrast, thermalizing umklapp processes are entirely frozen out, and the propagation is assumed to be predominantly governed by wave-vector-conserving anharmonic processes.

A quantity decisive for the mode of phonon propagation is the mean free path $\Lambda(T)$, and, in fact, $\Lambda(T)$ will be used to distinguish between the two regimes. Within the hot spot, $\Lambda(T)$ averaged over the phonon frequency may be derived from the thermal conductivity $\kappa(T)$ (Ref. 20) and the specific heat $C_V(T)$ (Ref. 21) by use of the relation

$$\kappa(T) = \tfrac{1}{3} C_V(T) v \Lambda(T) . \tag{1}$$

At the typical powers of 0.5 W, the temperature in the center of the hot spot reaches 1000 K, corresponding to $\Lambda(T) \approx 1$ nm (Fig. 3). However, $\Lambda(T)$ rapidly increases with decreasing temperature. The radius R_0 of the hot spot may therefore be estimated with reasonable accuracy from the criterion

$$R_0 = \Lambda(T_0) . \tag{2}$$

To work this out, it is further assumed that the power P injected into the crystal passes through the surface of the hemisphere without noticeable loss, and from there proceeds at the Debye velocity v (≈ 6 km/s). Under the stationary conditions of the experiment, then,

$$P = \tfrac{1}{4} \pi R_0^2 v \rho(T_0) , \tag{3}$$

where $\rho(T_0)$ is the phonon energy density at temperature T_0. Note that $\rho(T_0)$ can be obtained from integration of $C_V(T)$ over the temperature. Given P, R_0 can now be derived from Eq. (3) with an iterative procedure, in which T_0 is varied until consistency of Eqs. (1)–(3) is achieved. In Fig. 4 the resulting R_0 and T_0 are shown vs the power. Typical values for R_0 range from 3 to 10 μm. Self-evidently, if P is such that the calculated R_0 undershoots the radius R_{pc} of the point contact (≈ 3 μm), R_0 should be set equal to R_{pc}. As for T_0, it only weakly diminishes with P, obviously because of the sharp decrease in the mean free path around this temperature. The associated reduction of $\rho(T_0)$ is, however, strong enough to make R_0 increase approximately linearly with P.

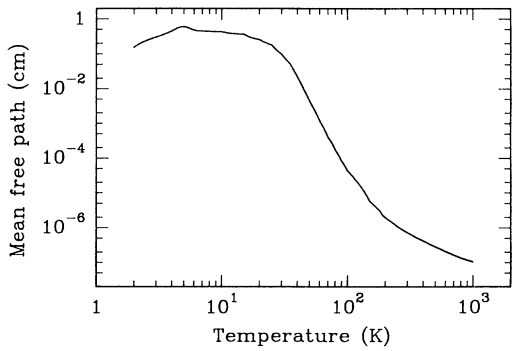

FIG. 3. The average phonon mean free path Λ vs the temperature.

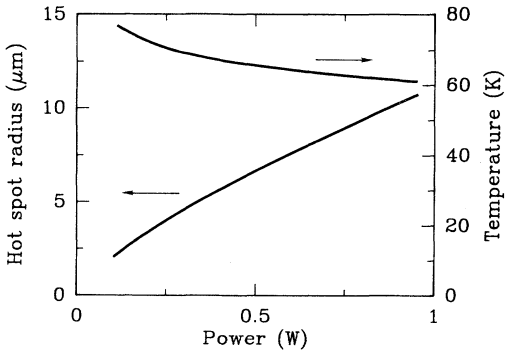

FIG. 4. The radius R_0 and surface temperature T_0 of the hot spot vs the power P injected into the ruby crystal.

Within the hemisphere the temperature profile was obtained by numerical integration of the classical equation for heat conduction,

$$\kappa(T)\frac{dT}{dr}=-\frac{P}{2\pi r^2}\ . \tag{4}$$

Beyond R_0, quasiballistic motion is assumed to prevail. In this regime, the phonon spectrum was, for reasons of tractability, approximated by a set of 6 Einstein modes with frequencies increasing by factors of 2, i.e., $\nu_i=2^i\nu_0$ $(i=0,1,\ldots,5)$. These modes are given weights proportional to the Debye density of states integrated from one midfrequency between these modes to the next. Their weights accordingly scale with ν_i^3. However, the upper limit of the frequency interval associated with the $i=5$ mode is set equal to the Debye frequency, and the lower limit of the $i=0$ mode is taken to extend to 0. The occupation numbers n_i of the Einstein modes thus represent the intrinsic phonon occupation per mode averaged over the ith interval. This procedure, which is equivalent to representing the density of states as a function of frequency by a series of rectangles of increasing widths covering the entire acoustic phonon energy band, is due to Schaich.[15] We take $\nu_2=0.87$ THz, corresponding to the phonon resonance frequency of excited Cr^{3+} in ruby.

Each mode ν_i is taken to propagate ballistically at the Debye velocity v, and is subjected to down-conversion to $\nu_i/2$ and up-conversion to $2\nu_i$ at rates proportional to ν_i^5. That is, at $r=R_0$, the occupation numbers n_i are set equal to the values pertaining to the temperature of the outer surface of the hot spot,

$$n_i(R_0)=[\exp(h\nu_i/kT_0)-1]^{-1}\ , \tag{5}$$

and their subsequent development as a function of the distance obeys the set of equations

$$v\left[\frac{\partial n_i(r)}{\partial r}+\frac{2n_i(r)}{r}\right]=\left.\frac{\partial n_i(r)}{\partial t}\right|_{\text{anh}}\ , \tag{6}$$

in which

$$\begin{aligned}\left.\frac{\partial n_i(r)}{\partial t}\right|_{\text{anh}}=&-R_i^-\{n_i(r)[1+n_{i-1}(r)]^2\\&-[1+n_i(r)]n_{i-1}(r)^2\}\\&+bR_i^+\{n_{i+1}(r)[1+n_i(r)]^2\\&-[1+n_{i+1}(r)]n_i(r)^2\}\ .\end{aligned} \tag{7}$$

Here, $R_{i-1}^+=R_i^-=R_0(\nu_i/\nu_0)^5$, where R_0 is chosen such that the anharmonic decay time $1/R_2^-$ of 0.87-THz phonons equals 1 μs.[22] Furthermore, $R_5^+=R_0^-=0$, because phonons of mode $i=5$, having a frequency $2^3\times0.87$ THz, cannot combine, and the decay of phonons of mode $i=0$, having a frequency $2^{-2}\times0.87$ THz, is ignored. The quantity b is set equal to 2^4 to ensure energy conservation during breakup. Here, a factor of 2^3 accounts for the weight of the Einstein mode $i+1$ relative to mode i, and another factor of 2 is due to the fact that a phonon of mode $i+1$ breaks up into 2 phonons of mode i.

V. PHONON-INDUCED WIDTH AND SHIFT OF $\bar{E}(^2E)$

We subsequently consider the phonon-induced shift δE and width $\Delta\nu$ of the $\bar{E}(^2E)$ level of the Cr^{3+} centers as a function of the distance-dependent phonon occupation. In good approximation, δE scales with the energy stored in the lattice.[23] We thus have

$$\delta E=\frac{\beta\Delta}{\nu_D^3}\mathcal{P}\int_0^{\nu_D}\frac{\nu^3n(\nu)}{\nu^2-\Delta^2}d\nu+\frac{\alpha'}{\nu_D^4}\int_0^{\nu_D}\nu^3n(\nu)d\nu\ , \tag{8}$$

where $\mathcal{P}$ denotes taking the principal value of the integral. With regard to $\Delta\nu$, it is noted that, except at very low phonon densities, the dephasing of $\bar{E}(^2E)$ is governed by phonon processes connecting $\bar{E}(^2E)$ with $2\bar{A}(^2E)$.[16] At low temperatures, $\Delta\nu$ is therefore determined by direct processes between $\bar{E}(^2E)$ and $2\bar{A}(^2E)$. At higher temperatures, however, Raman processes connecting $\bar{E}(^2E)$ and $2\bar{A}(^2E)$ dominate the width of $\bar{E}(^2E)$. Both contributions can be calculated by use of perturbation theory up to second order. In the Debye approximation of the density of states, and with inclusion of the $2\bar{A}(^2E)$ level, the homogeneous width can be written

$$\Delta\nu=\Delta\nu_0+\frac{\pi\beta}{\nu_D^3}\Delta^3n(\Delta)+\frac{\alpha}{\nu_D^7}\int_0^{\nu_D}\nu^6n(\nu)[n(\nu)+1]d\nu\ , \tag{9}$$

in which $n(\nu)$ is the phonon occupation at frequency ν, Δ is the $\bar{E}(^2E)-2\bar{A}(^2E)$ resonance frequency, α and β contain the matrix elements for Raman and direct processes, respectively, ν_D is the Debye cutoff frequency, and $\Delta\nu_0$ is the residual width at low temperatures (<10 K). The latter is determined by the hyperfine interactions between the Cr^{3+} electron spin and the surrounding Al nuclear spins, whose fluctuating magnetic field at the Cr^{3+} site modulates the R_1 resonance frequency through a dynamic Zeeman effect. From previous FLN and hole-burning experiments,[24] this width is known to be 65 MHz in zero magnetic field.

In evaluating Eqs. (8) and (9) at a given distance from the point contact, we have made use of the subdivision of the phonon density of states into rectangular packets, as discussed above, while the phonon occupations $n(\nu)$ have been set to $n_i(r)$, as appropriate. The remaining integrations have been carried out exactly over each packet. This procedure ensures that the Einstein modes are properly weighted. Calibrations for α and α' have been obtained by McCumber and Sturge[16] from the development of the R_1 luminescence as a function of temperature. For thermal phonon populations, Eqs. (8) and (9) become[16,25]

$$\delta E(T)=\beta\frac{T_\Delta}{T_D}\left[\frac{T}{T_D}\right]^2\mathcal{P}\int_0^{T_D/T}x^3n(x)\frac{1}{x^2-(T_\Delta/T)^2}dx + \alpha'\left[\frac{T}{T_D}\right]^4\int_0^{T_D/T}x^3n(x)dx\ , \tag{10}$$

$$\Delta\nu(T)=\Delta\nu_0+\pi\beta\left[\frac{T_\Delta}{T_D}\right]^3 n(\Delta) + \alpha\left[\frac{T}{T_D}\right]^7\int_0^{T_D/T}x^6n(x)[n(x)+1]dx\ , \tag{11}$$

where $T_D=h\nu_D/k_B$, $T_\Delta=h\Delta/k_B$, and $n(x)=(e^x-1)^{-1}$. As it turns out, the α parts, which are associated with Raman processes, indeed predominate in the high-temperature regime. The β terms are only 2% of their α counterparts at 150 K, and less than 1% at 300 K. The α and β terms in $\Delta\nu(T)$ balance at approximately 60 K. In $\delta E(T)$, the α part already predominates at temperatures as low as 20 K. McCumber and Sturge,[16] analyzing the temperature-dependent width of the inhomogeneous R_1 luminescence above 90 K on the basis of Eq. (11), found $\alpha=544\ \text{cm}^{-1}$ and $T_D=760$ K. From the data on $\delta E(T)$ at temperatures extending to 700 K, they further found $\alpha'=-400\ \text{cm}^{-1}$ by use of Eq. (10), again with neglect of the β part. The high-temperature data do not permit a determination of β. The contribution of the direct process can, however, be discerned when the inhomogeneous broadening of the optical transition is eliminated by the use of FLN.[19] The result is $\pi\beta(T_\Delta/T_D)^3=235\pm20$ MHz or $\beta=14.45\pm1.2\ \text{cm}^{-1}$.

VI. DISCUSSION

Images of the luminescence emanating from right under the point contact, as exemplified in Fig. 2, have been recorded following selective narrow-band laser excitation of Cr^{3+} to $\bar{E}(^2E)$ and the application of electrical power under cw conditions. Images of good quality could be obtained for laser frequencies displaced as far as $\delta\nu_l=32$ GHz below the central low-temperature $^4A_2-\bar{E}(^2E)$ transition. The results for the extent of the luminescent region below the hot spot have been collected in Fig. 5 as a function of the detuning $\delta\nu_l$. Note again that a larger detuning corresponds to a higher phonon occupation.

To analyze these data we resort to the procedure outlined in Sec. IV. First, R_0 and T_0 are evaluated from Eq. (3) in conjunction with the criterion equation (2) for the relevant $P\approx0.5$ W, with the results $R_0=7$ μm and $T_0=65$ K. Next, the set of six coupled differential equations (6) with the boundary condition equation (5) is solved numerically in the quasiballistic regime, to obtain $n_i(r)$ for $r\geq R_0$. In the regime of classical heat conduction, the increase of $n_i(r)$ toward lower r is calculated from Eq. (4). The resultant $n_i(r)$, displayed in Fig. 6, are subsequently entered into the evaluation of δE and $\Delta\nu$ [Eqs. (8) and (9)], again for various radii of the sphere around the point contact. At $r=R_0$, corresponding to a phonon distribution thermalized according to T_0, for example, δE appears to amount to 24 GHz, while $\Delta\nu$ equals 18 GHz. It should be recalled at this point, however, that the $^4A_2-\bar{E}(^2E)$ transition is inhomogeneously broadened. This entails an additional spread in δE, which, for tractability, is given a rectangular shape. The inhomogeneous spread amounts to 3 GHz full width for 700 at. ppm Czochralsky ruby. In order to arrive at the R_1 luminescent profiles for a given laser detuning $\delta\nu_l$, it is sufficient to evaluate the absorption probability as a function of r. If it is assumed that the phonon-induced line shape is Lorentzian, the absorption probability per unit of volume scales with

$$\frac{2/\pi\Delta\nu}{1+[2(\delta E-\delta\nu_l)/\Delta\nu]^2}\ , \tag{12}$$

convoluted with the inhomogeneous spread of δE. The absorption is clearly a function of r through δE and $\Delta\nu$, and, in fact, a luminescent hemispherical shell with a thickness of about one-third of the radius results. In line with the definitions of the extent of the experimental

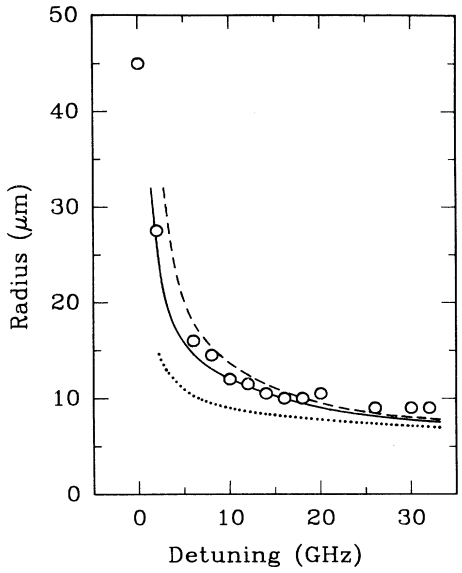

FIG. 5. The radius of the luminescent spot vs the detuning $\delta\nu_l$ to lower frequency. Solid curve represents a model calculation for a point-contact power of 0.5 W, and a point-contact size of 3 μm. Dashed curve applies to purely ballistic propagation, dotted curve to quasidiffusion.

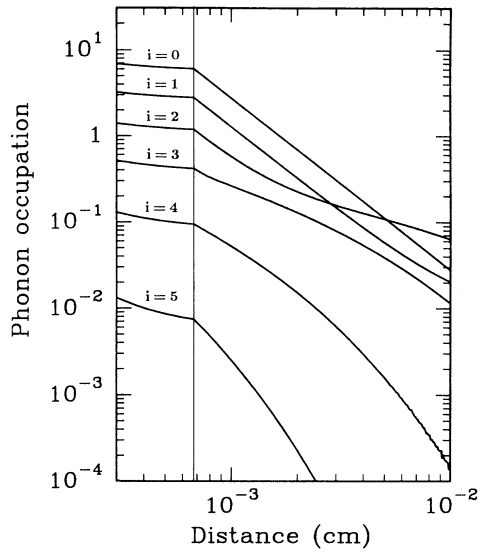

FIG. 6. The calculated phonon occupation numbers vs the distance for the six modes labeled $i=0,1,\ldots,5$ in the two regimes of propagation.

luminescent spot (cf. Sec. III), we finally take the outer half-value radius of this shell to represent the radius of the calculated luminescent region.

The results vs $\delta\nu_l$ are entered in Fig. 5 as the solid curve. Good agreement with experiment is found. In particular, the slow rise toward small detuning is adequately reproduced. At the largest $\delta\nu_l$, the luminescent radius appears to amount to about 9 μm, only slightly larger than the hot-spot radius R_0, where phonon occupations are still near those pertaining to T_0. The radius has increased to approximately $2R_0$ at $\delta\nu_l \approx 8$ GHz and to $4R_0$ at $\delta\nu_l \approx 2$ GHz. For smaller detuning, the radii are less reliable because of the inhomogeneous spread of δE. The data point of $\delta\nu_l = 0$ GHz is, in fact, determined by the finite waist of the laser beam. In order to obtain coincidence of the model with the data, we adjusted P. Coincidence was obtained for $P=0.5$ W, which was anticipated above. (In the quasiballistic regime, the luminescent radius scales roughly with $P^{1/2}$.) This value is about a factor of 2 smaller than the electrical power dissipated in the point contact, but certainly not outside the experimental errors combined with the uncertainties associated with the simplifying assumptions in the model.

It is of considerable interest to examine to what extent the results presented in Fig. 5 distinguish quasiballistic propagation beyond the limits of the hot spot from pure ballistic flight, on the one hand, and quasidiffusive motion on the other. To treat pure ballistic motion, we have repeated the calculation with the right-hand side of Eq. (6) set to zero, but otherwise the same parameters. The results of these calculations, entered in Fig. 5 as the dashed line, indicate that at larger distances from the contact the phonon energy stored in the modes of the highest frequency, which contribute the most to δE and $\Delta\nu$, is overestimated. Indeed, for pure ballistics all $n_i(r)$ drop with the squared distance, whereas at the relevant distances quasiballistic propagation invokes a notable down-conversion of the highest-frequency modes (cf. Fig. 6). To estimate the effects of quasidiffusive motion, we first note that in particular the energy propagating in the higher frequency modes is substantially delayed because the mean free path as determined by elastic scattering scales with ν^4. To mimic quasidiffusive motion in the framework of the model of Sec. IV, therefore, one may make v dependent on the mode number i. Reducing v for $i=4$ and 5 by a factor of 10, for example, we find a hot-spot size that is substantially more weakly dependent on the detuning $\delta\nu_l$ than observed, i.e., the edge of the hot spot is too abrupt (dotted curve in Fig. 5). In summary, therefore, quasiballistic propagation with an anharmonic decay time of 1-THz phonons of order 1 μs appears to provide an adequate description of the data.

VII. COMPARISON WITH FLN EXPERIMENTS

Another stringent test of our model is provided by the spectrum of the R_1 luminescence rather than by its spatial extent. This spectrum was recently measured with high resolution by the use of the technique of fluorescence line narrowing (FLN), but for reasons of sensitivity the data were integrated over the entire luminescent region.[19] In FLN experiments, as in the present ones concerned with optical imaging of the luminescent region, a homogeneous packet within the inhomogeneously broadened line is selectively excited with a narrow-band laser, but the ensuing luminescence is analyzed with high spectral resolution.

In the experiments of Ref. 19, excitation of Cr^{3+} to $\bar{E}(^2E)$ was achieved with a narrow-band laser (1 MHz), and high spectral resolution of the detection was provided by a temperature-stabilized piezo-scanned Fabry-Perot interferometer in combination with a 0.85-m double monochromator. The luminescence emanating from below the point contact was collected at right angles, and imaged onto a pinhole in front of the interferometer. This, in effect, amounted to integrating the luminescence from all shells about the point contact up to radii of 100 μm. Further, the use of an add-subtract scheme permitted to obtain the *modification* of the R_1 luminescence by the phonons injected by the point contact.

The results are reproduced in Fig. 7 for three values of the laser detuning, where positive contributions arise from homogeneous packets shifted to resonance with the laser, and thus are broadened (cf. Sec. V). The central negative contribution, on the other hand, results from homogeneous packets that are shifted out of resonance. To compare our model with the FLN measurements, we have calculated the emitted luminescence spectrum as follows. (i) The phonon distribution versus distance from the point contact is calculated according to Sec. IV; (ii) the shift δE and the width $\Delta\nu$ of the $\bar{E}(^2E)-2\bar{A}(^2E)$ transition are calculated versus distance, as in Sec. V; (iii) the spectrum emitted by each contributing shell is assumed to be a Lorentzian of width $\Delta\nu$, centered around the laser frequency ν_l; (iv) the absorption probability for single-frequency light at a given distance is assumed to

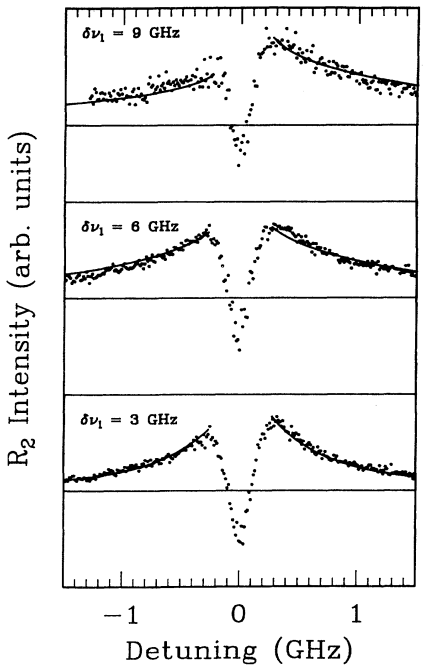

FIG. 7. Fluorescence line-narrowing spectra for various detunings $\delta\nu_l$ of the laser, showing phonon-induced broadening of the R_1 luminescence. Solid lines correspond to a model calculation for an injected power of 1 W. The negative contributions are inherent to the experimental method, and should be disregarded here.

scale linearly with a Lorentzian of width $\Delta\nu$ centered around δE [cf. Eq. (12)];[26] (v) the luminescence spectrum is obtained by summation of all contributing shells weighted according to their volumes. In this procedure we have ignored the inhomogeneous width, as we are concerned with laser detunings that are significantly larger. We have further disregarded the negative central part, extending to 0.25 GHz on either side in the spectra. In Fig. 7, calculated curves are presented for a point-contact power of 1 W. These curves faithfully track the data, thereby providing substantial further justification of the hot-spot model as well as the approximations made.

VIII. CONCLUDING REMARKS

A hot spot of several hundreds of Kelvin and of a size of a few micrometers has been generated in ruby upon injecting high phonon fluxes (up to 3×10^{10} W/m^2) with a whisker-film point contact. Further, it has been shown that excitation of Cr^{3+} in ruby to $\bar{E}(^2E)$ in a way that is selective for the phonon energy density combined with direct optical imaging of the ensuing luminescence is a powerful means of investigating hot spots. The experimental scheme permits direct access to the phonons emitted by the hot spot over considerable distances and with high spatial resolution. In ruby, the applicability is constrained by inhomogeneous broadening of the $^4A_2-\bar{E}(^2E)$ transition and by homogeneous broadening induced by the phonons. The former limits the selectivity in the cool areas of the crystal, where δE is masked by the inhomogeneous spread, whereas the latter leads to a reduction of the resolution and the luminescent intensity close to the hot spot. A model description of the phonon distribution near the point contact in terms of classical heat conduction close to the point contact and a contiguously surrounding regime of quasiballistic propagation further away appears to be in good accord with the data. The phonons, which initially had frequencies up to the zone boundary, are subjected to notable net down-conversion. The model developed also faithfully describes fluorescence line-narrowing data.

ACKNOWLEDGMENTS

The authors thank C. R. de Kok for invaluable technical assistance. The work was financially supported by the Netherlands foundation "Fundamenteel Onderzoek der Materie" and the "Nederlandse Organisatie voor Wetenschappelijk Onderzoek."

[1]Y. B. Levinson, in *Nonequilibrium Phonons in Nonmetallic Crystals,* edited by W. Eisenmenger and A. A. Kaplyanskii (Elsevier, Amsterdam, 1986), p. 91.

[2]D. V. Kazakovtsev and Y. B. Levinson, in *Physics of Phonons,* proceedings of the XXIIIth Winter School of Theoretical Physics, Karpacz, 1987, edited by T. Paszkiewicz, (Lecture Notes in Physics, Vol. 285) (Springer, Berlin, 1987), p. 276.

[3]J. C. Hensel and R. C. Dynes, Phys. Rev. Lett. **39**, 969 (1977).

[4]M. Greenstein, M. A. Tamor, and J. P. Wolfe, Phys. Rev. B **26**, 5604 (1982).

[5]A. V. Akimov, A. A. Kaplyanskii, M. A. Pogarskii, and V. K. Tikhomirov, Pis'ma Zh. Eksp. Teor. Fiz. **43**, 259 (1986) [JETP Lett. **43**, 333 (1986)].

[6]A. V. Akimov, A. A. Kaplyanskii, and E. S. Moskalenko, Fiz. Tverd. Tela (Leningrad) **29**, 509 (1987) [Sov. Phys. Solid State **29**, 288 (1987)].

[7]A. V. Akimov, A. A. Kaplyanskii, V. I. Kozub, P. S. Kop'ev, and B. Ya. Mel'tser, Fiz. Tverd. Tela (Leningrad) **29**, 1843 (1987) [Sov. Phys. Solid State **29**, 1058 (1987)].

[8]V. S. Bagaev, G. Bel'skaya-Levandovskaya, M. M. Bonch-Osmolovskii, T. I. Galkina, S. Yu. Levandovskii, G. N. Mikhailova, A. G. Poyarkov, and G. Jung, Zh. Eksp. Teor. Fiz. **77**, 2117 (1979) [Sov. Phys.—JETP **50**, 1013 (1979)].

[9]N. N. Zinov'ev, D. N. Kovalev, V. I. Kozub, and I. D. Yaroshetskii, Zh. Eksp. Teor. Fiz. **92**, 1331 (1987) [Sov. Phys.—JETP **65**, 746 (1987)].

[10]W. E. Bron, J. L. Patel, and W. L. Schaich, Phys. Rev. B **20**, 5395 (1979).

[11]A. P. Abramov, I. N. Abramova, I. Ya. Gerlovich, and I. K. Razumova, Zh. Eksp. Teor. Fiz. **92**, 666 (1987) [Sov. Phys.—JETP **65**, 376 (1987)].

[12]W. Eisfeld and K. F. Renk, Appl. Phys. Lett. **34**, 481 (1979).
[13]This is confirmed by the observations of melting of point contacts made of Au (melting point 1336 K) when applying pulses of over 1 W. Electron micrographs of W-W point contacts indicate heating over areas of order 3 μm in diameter.
[14]V. I. Kozub, Zh. Eksp. Teor. Fiz. **94**, 186 (1988) [Sov. Phys.—JETP **67**, 1191 (1988)].
[15]W. L. Schaich, Solid State Commun. **49**, 55 (1984); T. E. Wilson and W. L. Schaich, *ibid.* **50**, 3 (1984).
[16]D. E. McCumber and M. D. Sturge, J. Appl. Phys. **34**, 1682 (1963).
[17]G. F. Imbusch and S. Geschwind, in *Optical Properties of Ions in Crystals,* edited by H. M. Crosswhite and H. W. Moos (Wiley, New York, 1967), p. 171.
[18]A. Szabo, Phys. Rev. B **11**, 4512 (1975).
[19]M. J. van Dort, K. Z. Troost, J. I. Dijkhuis, and H. W. de Wijn, J. Phys. Condens. Matter **2**, 6721 (1990).
[20]Y. S. Touloukian, R. W. Powell, C. Y. Ho, and P. G. Klemens, *Thermal Conductivity-Nonmetallic Solids, Thermophysical Properties of Matter,* edited by Y. S. Touloukian and C. Y. Ho (Plenum, New York, 1970), Vol. 2.
[21]Y. S. Touloukian and E. H. Buyco, *Specific Heat-Nonmetallic Crystals, Thermophysical Properties of Matter,* edited by Y. S. Touloukian and C. Y. Ho (Plenum, New York, 1970), Vol. 5.
[22]R. Baumgartner, M. Engelhardt, and K. F. Renk, Phys. Rev. Lett. **47**, 1403 (1981).
[23]G. F. Imbusch, W. M. Yen, A. L. Schawlow, D. E. McCumber, and M. D. Sturge, Phys. Rev. **133**, A1029 (1964).
[24]P. E. Jessop, T. Muramoto, and A. Szabo, Phys. Rev. B **21**, 926 (1980).
[25]B. Di Bartolo, *Optical Interactions in Solids* (Wiley, New York, 1968), p. 367.
[26]The linewidth of the luminescence observed in an FLN experiment is double the width of the homogeneous packet.